Research article

Frequency regulation of interconnected hybrid power system with Assimilation of electrical vehicles

Amil Daraz [a], Irfan Ahmed Khan [b], Abdul Basit [a], Suheel Abdullah Malik [c], Salman A. AlQahtani [d], Guoqiang Zhang [a,*]

[a] School of Information Science and Engineering, NingboTech University, Ningbo 315100, China
[b] Department of Electrical Engineering, Faculty of Engineering, Universiti Malaya, 50603 Kuala Lumpur, Malaysia
[c] Department of Computer and Electrical Engineering, FET, International Islamic University, Islamabad 44000, Pakistan
[d] Computer Engineering Department, College of Computer and Information Sciences, King Saud University, Riyadh, Saudi Arabia

ARTICLE INFO

ABSTRACT

Recent widespread connections of renewable energy resource (RESs) in place of fossil fuel supplies and the adoption of electrical vehicles in place of gasoline-powered vehicles have given birth to a number of new concerns. The control architecture of linked power networks now faces an increasingly pressing challenge: tie-line power fluctuations and reducing frequency deviations. Because of their nature and dependence on external circumstances, RESs are analogous to continually fluctuating power generators. Using a fractional order-based frequency regulator, this work presents a new method for improving the frequency regulation in a two-area interconnected power system. In order to deal with the frequency regulation difficulties of the hybrid system integrated with RES, the suggested controller utilizes the modified form of fractional order proportional integral derivative (FOPID) controller known as FOI-PDN controller. The new proposed controllers are designed using the white shark optimizer (WSO), a current powerful bioinspired meta heuristic algorithm which has been motivated by the learning abilities of white sharks when actively hunting in the environment. The suggested FOI-PDN controller's performance was compared to that of various control methodologies such as FOPID, and PID. Furthermore, the WSO findings are compared to those of other techniques such as the salp swarm algorithm, sine cosine algorithm and fitness dependent optimizer. The recommended controller and design approach have been tested and validated at different loading conditions and different circumstances, as well as their robustness against system parameter suspicions. The simulation outcomes demonstrate that the WSO-based tuned FOI-PDN controller successfully reduces peak overshoot by 73.33%, 91.03%, and 77.21% for region-2, region-1, and link power variation respectively, and delivers minimum undershoot of 89.12%, 83.11%, and 78.10% for both regions and tie-line. The obtained findings demonstrate the new proposed controller's stable function and frequency controlling performance with optimal controller parameters and without the requirement for a sophisticated design process.

* Corresponding author.
  E-mail address: guoqiang_zhang@nbt.edu.cn (G. Zhang).

List of nomenclature and notation

Acronym Definition

IPS	Interconnected Power System
LFC	Load Frequency Control
WSO	White Shark Optimization
ACO	Ant Colony Optimization
RES	Renewable Energy Sources
SLP	Step Load Perturbation
FDO	Fitness Dependent Optimizer
ΔF	Frequency Deviation
PID	Proportional Integral Derivative
SCA	Sine Cosine Algorithm
ABC	Artificial Bee Colony
PIDF	Proportional-Integral-Derivative Filter
ITAE	Integral Time Absolute Error
ISE	Integral Square Error
ANN	Artificial Neural networks
TIDN	Tilt integral derivative with filter
FLC	Fuzzy Logic Control
FO	Fractional Order
TF	Transfer Function
TD	Time Delay
BD	Boiler Dynamic

Acronym Definition

ΔP_D	Load Deviation
R	Speed Regulation
ΔP_G	Output deviation of a generator
ΔF	Frequency Deviation
T_p	Time Constant of Power System
MO	Maximum Overshoot
K_{pv}	Photovoltaic Constant
K_{pv}	Photovoltaic Constant
M	Inertia Constant
ST	Settling time
MU	Maximum Undershoot
H	Power System Gain
MG	Microgrid
HMG	Hybrid Microgrid
ΔX_G	Valve Position of Governor
U_b	Upper Boundary
ITSE	Integral Time Square Error
T_w	Wind Time Constant
L_b	Lower Boundary
K_{wave}	Gain of wave energy
GRC	Generation Rate constraint
GDB	Governor Deed Band

1. Introduction

1.1. Background

Modern installations and broad adoption of numerous new clean RESs have become more critical answers to climate change [1]. In recent years, the RES energy shift has grown to be commonplace [2]. Consequently, the number of installations using power electronic-based converters to connect renewable energy systems to conventional power grids has increased. In contrast to conventional generating systems that don't use power electronic converters, RES that rely on power electronics have reduced power system inertia [3]. Modern power systems built on RESs as a result have less PS inertia, and their values decrease as more RESs are included into power systems. Due to the absence of the rotating masses found in conventional generation systems, the cumulative power

systems' inertia is thus significantly decreased. In comparison to conventional non-renewable energy sources, this causes frequency stability to deteriorate and adds significant frequency spikes. As a result, stability, reliability, and security issues have been raised by the extreme breach levels of RESs in contemporary electrical power networks [4,5].

The control system must lessen frequency alterations in each location and limit power tie-line changes in order to handle unanticipated disturbances in contemporary power systems [6]. Typically, the load frequency control (LFC) of an IPS is referred to as this activity. The existing speed governors are used to implement the primary functions of LFC. However, speed governors alone are unable to effectively mitigate the tie-line fluctuations in frequency and power that occur in modern power networks based on renewable energy sources. The speed governors are unable to adequately balance the power production and load necessity. As a consequence, it is essential for the researchers to use the proper control methods, and to improve their design strategies in order to minimize or eliminate the sustained frequency deviations of each area, as well as the corresponding power deviations from the tie-lines [7].

1.2. Literature review

There are various study recommendations for integrating EVs in the LFC in the literature [8,9]. However, with an interconnected multi-area PS, the complexity of managing EVs with the current LFC approaches has emerged as a difficult problem. Numerous integrated orders, model predictive control (MPC), neural network (NN), fuzzy logic controller (FLC), fractional order (FO) and intelligent control systems have been proposed as optimum controllers for LFC in the literature [10–13]. The literature has extensively merged the various control elements using the derivative (D), tilt (T), integrator (I), proportional (P), and derivative filter (F) to construct various LFC systems. For EVs, the PI controller has been introduced in Ref. [14]. However, this controller has stability problems, particularly when taking into account the communication system's time delays.

The authors in Ref. [15], the FOPID with FO filter was proposed, and the SCA technique was used to effectively optimize the parameters of the suggested controller. In Ref. [16], the Harris Hawks Optimization (HHO) algorithm was used to optimally construct the PI LFC settings. Daraz et al., in Ref. [17] used FOTIDN for multisource IPS considering various non linearities with the inclusion of capacitive energy storage. The parameters of the proposed algorithm are adjusted by hybrid SCA with FDO. The authors in Ref. [18] utilized TID controllers and adjusted the coefficients of the anticipated controller employing a heuristic approach based on bee colony optimization. Particle swarm optimization was also used during the development of the virtual inertia control system described in Ref. [19]. Zhang et al. in Ref. [20] suggested well-tuned cascaded PI-PDF controllers using the driver training-based optimization, for a hybrid PS. In Ref. [21], the chaotic butterfly optimization algorithm was presented for adjusting the PI-TID controller. To address the AGC difficulties in linked PS, an enhanced FFOID controller with energy storage device has been introduced in Ref. [22]. The path finder optimization technique (PFA) has also been used to offer an optimized design for the TID controller [23]. Sahoo et al. [24] has recommended a green leaf-hopper flame algorithm to tune the gains of the proposed controllers. The researchers in Ref. [25] employed a 2-degree-of-freedom (2DOF)-PI controller based on heuristic computational strategies. This controller effectively manages the voltage output of synchronous generators, particularly in the face of significant and continuous disturbances. Similarly, Mohapatra et al. [26] employed a 2DOF-FOPID controller for AGC of dual area power generation which has been optimized with a quasi-oppositional based SSA optimization technique.

The slap swarm optimization algorithm, proposed in Ref. [27], has been used to optimize the combination of PI and TD controller with filter. In addition to a parallel sequence of TIDF, a hybrid strategy combining a modified PSO with the genetic algorithm (GA) was described for developing the regulator in Ref. [28]. For AGC systems, a better controller based on an imperialist competitive algorithm (ICA) optimized FOPI-FOPD controller has been recommended in Ref. [29]. When there are multiple step changes in the assembly and/or loading, the given controller can efficiently improve the performance of power systems. The FLC and FOPID are employed to achieve frequency adaptation in two-area power networks in Ref. [30]. For optimizing controller settings, the ICA has been developed. The authors of [31] anticipated a new technique to regulate the frequency in an individual self-regulating, and mix microgrid system, which comprises an energy storage unit, a solar gas turbine, a wind turbine generator, a biodiesel generator, and a DC connection using the TID controller. Additionally, it has been suggested to build the modified FO controller in IPS using the improved fitness determined optimization approach [32]. Amil et al. in Ref. [33] suggested well-tuned FOPID and MFOPID controllers using the jellyfish search optimizer (JSO) for a hybrid PS. Another use of the ICA optimizer for obtaining the best settings for the FTIDF-II controller for LFC systems was proposed in Ref. [34]. The researchers in Ref. [35] employed an ITDF controller to regulate the frequency of microgrid system employing Jaya algorithm (JA). Ravi et al. in Ref. [36] proposed FOPI controller combined with FO Proportional-Integral-Time Derivative (PTID) control, incorporating with energy storage devices to stabilize fluctuations in dual area interconnected PS. The authors in Ref. [37] applied a cascade FO fuzzy PID(FOFPID) with integral double derivative (IDD) controller for the effective optimization of tidal turbines. The tuning of the design variables for this controller was performed using the recently introduced Jaya algorithm. Nayak et al. in Ref. [38] employed a 2DOF optimal fuzzy PID controller for AGC of two and three area power generation which has been optimized with an adaptive crow search algorithm. The authors in Ref. [39] present a modified TID controller based on fractional order termed as FOI-TD that has been optimized using the improved FDO approach. In Ref. [40], the slap swarm optimizer (SSA) algorithm was presented for adjusting the PID controller. In addition, the butterfly optimization approach has been employed in Ref. [41] for the developing of the dual-stage PI-(1CID) controller. A FO-ID with a filter regulator is proposed in Ref. [42] for wind, fuel cell, and solar AGC systems.

1.3. Motivation and Research Gap

It is now obvious that the literature has a number of LFC ideas using different optimization techniques. The performance of the
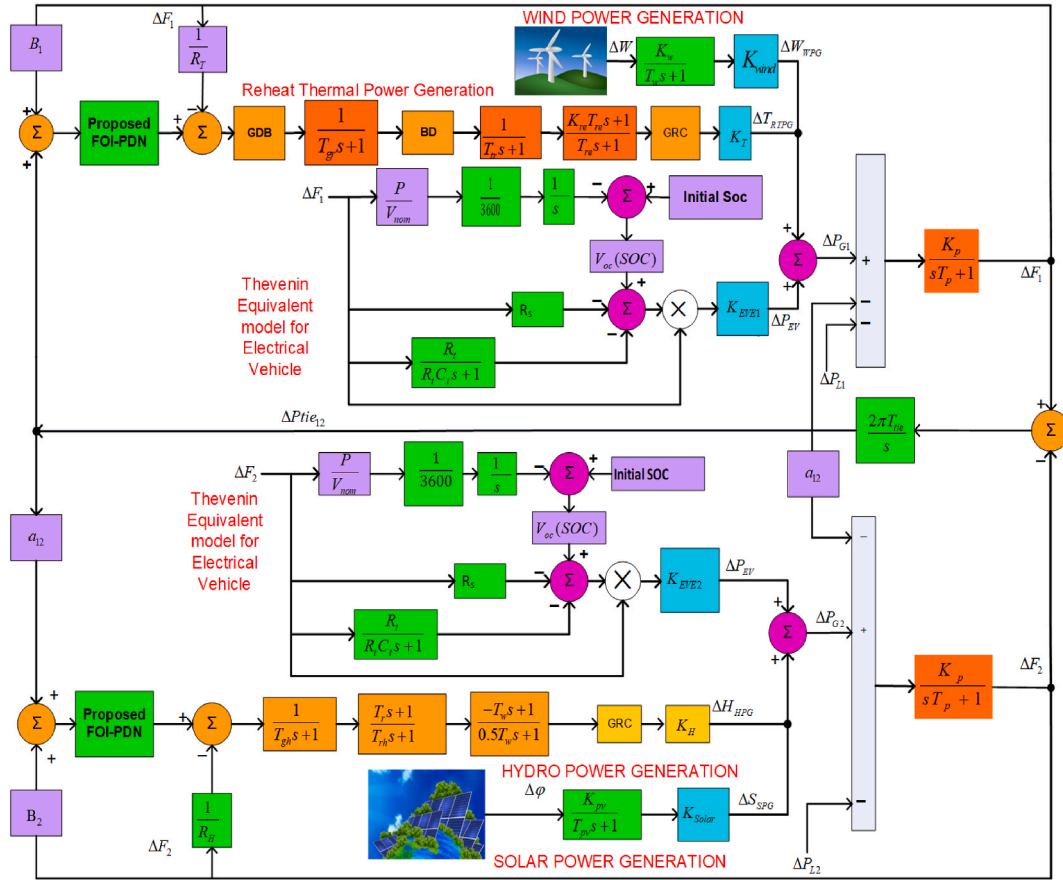
Fig. 1. Structure of hybrid power unit.

power grid during transients is largely determined by the pattern of the LFC category and the chosen optimizer. However, improved LFC technique performance and design approaches are required to reduce the anticipated burden impacts of RESs in forthcoming low-inertia power grids. This work describes a novel modified FO-LFC scheme that incorporates a cascaded configuration of PD, and FOI with filter. From a different perspective, their parameters require significant adjusting efforts. Due to their increased propensity to settle at local minimums, several metaheuristic optimizers methods are unreliable [43]. Additionally, acceptable adjusting is necessary for a number of parameters, particularly for FO- LFC techniques. As a result, the choice of parameter optimization raises significant difficulties [44]. Some optimizers further experience extended elapsed times, saturation, and high sensitivity to parameter changes. Long processing times are another drawback with some optimizers, necessitating multiple iterations to guarantee solution convergence.

This paper introduces the WSO method that was motivated by the learning abilities of white sharks when actively hunting in the environment. This algorithm was created by the authors of [45] with the goal of resolving practical optimization issues that are challenging to resolve with present techniques, both constrained and unconstrained. The recommended WSO has several advantages for complicated optimization challenges, including its projected malleability in handling various forms of optimization complications, because many types of problems require greater elasticity than WSO can stipulate. Moreover, due to the mathematical organization of WSO, it can be utilized to solve a wide range of industrial challenges, specifically those with a high number of dimensions. It should be able to quickly and accurately discover the global optimal problems to difficult optimization problems due to its simplicity and durability [46,47].

1.4. Contribution and structure of the paper

The primary contributions of this study are outlined below grounded on the encouragement provided by the recent disruption in LFCs and their design methodologies.

- The cascade structure of the fractional order integrator (FOI) with proportional derivative with filter (PDN) is used for the two-area interconnected hybrid PS.
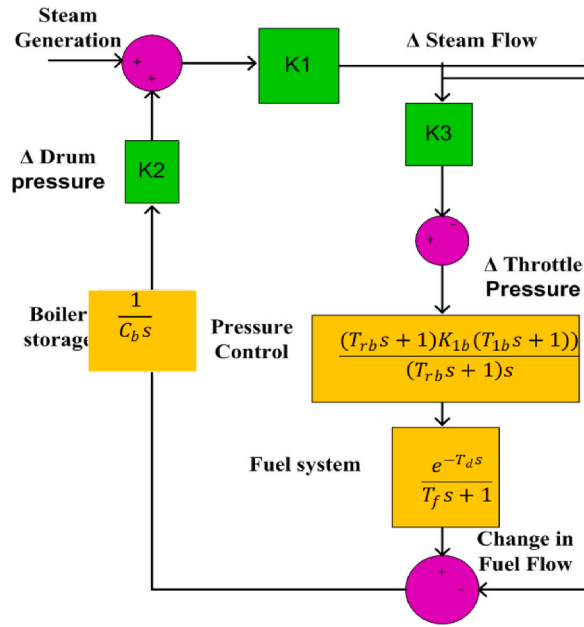
Fig. 2. Dynamical structure of the drum type boiler [20].

- Comparative analysis is performed between the suggested cascaded control structure and various cutting-edge control methodologies including FOPID, and PID controller. Furthermore, the white shark optimizer (WSO), which determines the parameters of the suggested controller in the best possible way, is used to improve the performance of the proposed LFC approach. The effectiveness of the WSO is further confirmed by comparisons with other current algorithms like SCA, SSA and FDO.
- The proposed hybrid power system has been analyzed with various non linearities to assure the practicality of the system.
- Finally, the suggested cascaded controller's resilience is validated using a load change of $\pm$ (25 %) and ($\pm$50 %), and parameters of the system within $\pm$ (30%) tolerance.

The rest of the article is drafted in the following manner: A description of the hybrid power system is given in Section 2, followed by a description of conventional and renewable power systems. In Section 3, the white shark optimization algorithm is demonstrated, while in Section 4, the control structure followed by the objection function is discussed. In section 5, the results and discussion are displayed which further elaborate the findings considering different scenarios. The final section of this paper discusses concluding remarks as well as future directions.

2. Power systems under study

Fig. 1 depicts the design of the proposed FOI-PDN controller employing the dual area PS with RESs and EVs. The RESs are spread throughout the zones, with PV energy installed in zone 1 and wind energy installed in zone 2. A hydropower plant is located in area 2, while the thermal unit is located in area 1. Furthermore, it is assumed that the distribution of EVs between the two regions is equal. Based on the PS material from Refs. [48,49], which are provided in Appendix A, the system is constructed in Matlab/Simulink. As a matter of fact, there is a limit to how much real power can be changed by thermal or hydro units. In other words, the devised LFC for an unconfined generation rate may not be reasonable in practice. In terms of both the rising and falling rates, the generation rate constraints (GRC) of 10%/min is taken into account for the thermal units. For the hydro unit, a typical GRC of 270%/min is taken into consideration for rising generation and 360%/min is taken into consideration for falling generation, respectively [50,51].

Equation (1) demonstrates the transfer function (TF) for governor dead zone/band (GDZ/GDB) [52]. While Equation (2) represents the values for N_2 [17].

$$\text{GDZ}\Big/\text{GDB} = \frac{N_1 + SN_2}{T_{sg}S + 1} \tag{1}$$

Where $N_1 = 0.8$ and,

$$N_2 = \frac{-0.2}{\pi} \tag{2}$$

Controller execution can be impacted by communication time delay (CTD), which can also enhance system oscillations. As a result, this study contains a simulation analysis that takes into account various system nonlinearities as well as CTD in the controller fault
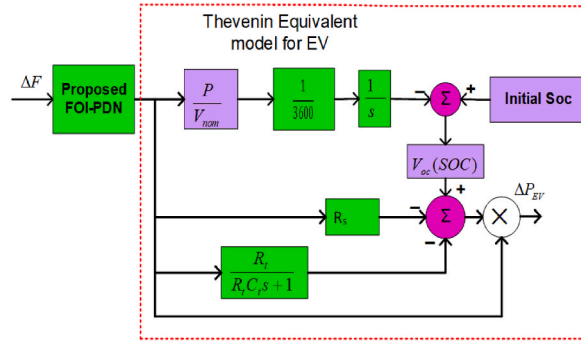
Fig. 3. Dynamic model of EV system [1].

domain. A TF model for the boiler dynamic (BD) is depicted in Fig. 2. Both efficiently managed coal/fired power units and inefficiently managed gas/oil fired power units can be analyzed using this paradigm. The relevant controls are promptly turned on when the boiler control system notices a change in pressure or steam flow rate. Traditional steam power plants modify their generation in this way. The TF model for BD is illustrated by Equations (3) and (4) [53,54]:

$$T_{cpu}(s) = \frac{K_{1b}(1 + T_{1b}s)(1 + T_{rb}s)}{(1 + 0.1T_{rb}s)s} \tag{3}$$

$$T_f(s) = \frac{e^{-t_d(s)}}{Ts + 1} \tag{4}$$

2.1. Modelling of EV systems

The performance of the PS can be efficiently controlled by the batteries of current EVs. Depending on what the management of the electrical PS requires, they can charge or discharge. They may result in better dynamic response, efficiency, and dependability of the power system, among other improvements. Because of the wavering nature of RES and the electrical demands associated with them, one of the most important tasks for their utilization is to contribute to the frequency stability of a PS. The dynamical model of EV systems used in this paper's frequency response study is shown in Fig. 3 [55].

Nernst equation relates open-circuit-voltage (Voc) to state-of- charge (SOC) for the linked EVs which has been specified in Equation (5) [54,55]:

$$V_{oc}(SOC) = S\frac{RT}{F}\ln\left(\frac{SOC}{C_{nom} - SOC}\right) + V_{nom} \tag{5}$$

where C_{nom} is the nominal capacity and V_{nom} is their nominal voltage of EV batteries. S represents sensitivity parameter, R, F and T signifies the gas, Faraday, and temperature constant respectively.

2.2. Modelling of conventional power systems

The governor $G_{TG}(s)$, the reheat ($G_{TR}(s)$), and the turbine (G_{TT} (s)) make up the overall TF for thermal generation ($G_T(s)$), which is characterized by Equations (6)–(9) respectively [50].

$$G_{TG}(s) = \frac{1}{(1 + T_{gr}s)} \tag{6}$$

$$G_{TR}(s) = \frac{1 + T_{re}K_{re}s}{(1 + T_{re}s)} \tag{7}$$

$$G_{TT}(s) = \frac{1}{(1 + T_{tr}s)} \tag{8}$$

$$G_T(s) = \frac{1 + T_{re}K_{re}s}{(1 + T_{gr}s)(1 + T_{re}s)(1 + T_{tr}s)} \tag{9}$$

Similarly, the combined TF of hydral power system ($G_H(s)$) is combined with the TF of the governor ($G_{HG}(s)$), TF of the penstock ($G_{HT}(s)$, and the TF of the droop compensation ($G_{HD}(s)$) which is represented by Equations (10)–(13), respectively [50].

$$G_{HG}(s) = \frac{1}{(1 + T_h s)} \tag{10}$$

$$G_{HT}(s) = \frac{(1 + T_{rs} s)}{(1 + T_{rh} s)} \tag{11}$$

$$G_{HD}(s) = \frac{(1 - T_w s)}{(1 + 0.5 T_w s)} \tag{12}$$

$$G_H(s) = \frac{(1 - T_w s)(1 + T_{rs} s)}{(1 + T_h s)(1 + 0.5 T_w s)(1 + T_{rh} s)} \tag{13}$$

2.2.1. RESs' models

A wind turbine is a device used to transform the kinetic energy of the wind into electrical energy. The, mechanical, aerodynamics, actuator, and electrical subsystems are the four subsystems that make up the entire wind turbine. The TF model $G_W(s)$ given in Equation (14) represents a wind plants [55,56]:

$$G_w(s) = \frac{K_w}{T_w s + 1} \tag{14}$$

Wind farm gain and time constant are denoted as K_w and T_w, respectively. A solar power generation system consists of a number of components, such as a photovoltaic plate, an inverter, a transformer, a boost converter and many others. The photovoltaic array is typically connected to a low-voltage DC capacitor, which allows the power output of the photovoltaic array to be modified by altering the voltage profile of the solar array, which in turn allows the power output to be modified. While the PV energy system model $G_{PV}(s)$, is represented in Equation (15) [55,56]:

$$G_{PV}(s) = \frac{K_{PV}}{T_{PV} s + 1} \tag{15}$$

where Kpv and Tpv are the gain and time constant of the PV plant, respectively.

3. White Shark optimization

WSO is recently proposed in Ref. [45], was inspired by the great white shark's behavior. Great white sharks are excellent predators and hunters, with keen eyesight, strong muscles, and a keen sense of smell. Numerous marine/non-marine organisms, such as mammals, amphibians, crustaceans, invertebrates, and seabirds, are among its prey. Sharks typically ambush their prey, hoping to catch its prey off guard before biting it in the deadly back. The more unusual senses of smell and hearing, as well as the ability to catch prey by swimming, that great sharks possess make their social behavior far more fascinating. The detail of WSO algorithm consists of the following steps.

3.1. Initialization

Since WSO is a population-based approach, it generates a collection of hypotheticals starting points for the optimization process. Equation (16) shows a population of N sharks (population range) in a d-dimensional (problem aspect), where the position of each shark represents a possible solution to a problem [46,47].

$$\begin{bmatrix} W_1^1 & W_2^1 & W_3^1 & \cdots & W_d^1 \\ W_1^2 & W_2^2 & W_3^2 & \cdots & W_d^2 \\ \vdots & \vdots & \vdots & \cdots & \vdots \\ W_1^N & W_2^N & W_3^N & \cdots & W_d^N \end{bmatrix} \tag{16}$$

Where w stands for each shark in the search area, d stands for the decision variables, and W_d^i stands for the position of the (ith) shark in the (dth) dimension. The initial population is determined using a uniformly random initialization, as shown in Equation (17) [45]:

$$W_j^i = r \times (u_j - l_j) + l_j \tag{17}$$

where W_j^i is the starting vector, l_j and u_j represent the lower and upper boundaries in the jth dimension, and r is a random number $\in$ (0,1).

3.2. Movement speed towards prey

Sharks use the delay in the tides they hear to reveal the setting of their prey, and their wavy motion can be described by equation

(18) [46].

$$V_{k+1}^i = \mu \left[V_k^i + P_1 \left(W_{gbest_k} - w_k^i \right) \times C_1 + P_2 \left(W_{best}^{i'k} - w_k^i \right) \times C_2 \right]$$

(18)

where V_{k+1}^i represents the updated velocity and V_k^i denotes the current velocity, $W_{best}^{i'k}$ is the swarm best location, w_k^i is the present position of the shark and W_{gbest_k} represents the global best position. C1 and C2 are the random numbers $\in (0,1)$. Similarly, P_1, P_2 (forces of white sharks), and μ (constriction factor) are represented by Equations (19)–(21) [46].

$$P_1 = P_{max} + (P_{max} - P_{min}) \times e^{-\left(\frac{4k}{K}\right)^2}$$

(19)

$$P_2 = P_{min} + (P_{max} - P_{min}) \times e^{-\left(\frac{4k}{K}\right)^2}$$

(20)

$$\mu = \frac{2}{\left| 2 - \tau - \sqrt{\tau^2 - 4\tau} \right|}$$

(21)

Where K = maximum no of iterations, k = current iteration. The initial and dependent velocities for white sharks are represented by P_{min} and P_{max}. Where τ is the acceleration coefficient, which was determined through careful analysis to be 4.125. The best position of the white shark is represented by Equation (22) [45].

$$v = [n \times rand(1,n)] + 1$$

(22)

3.3. Progress towards efficient prey

In this circumstance, the shark keeps moving to random locations in search of prey, much like a school of fish does. In this scenario, the proactive routing framework described in Equation (23) was used to characterize shark behavior as it approached prey [45].

$$w_{k+1}^i = \begin{cases} w_k^i. \neg \oplus w_0 + l.b + u.a; \ rand < mv \\ w_k^i + \dfrac{V_k^i}{f}; \ rand > mv \end{cases}$$

(23)

Binary vectors a and b are specified in Equations (24) and (25) respectively. While equation (26) represents the relation between a and b [45].

$$a = sgn\left(w_k^i - 1\right) > 0$$

(24)

$$b = sgn\left(w_k^i - 1\right) < 0$$

(25)

$$w_0 = \oplus (a, b)$$

(26)

White sharks are characterized by Equations (27) and (28), which explain the occurrence of the shark's curvy sign and the number of periods the crook strikes its object [45].

$$f = f_{min} + \frac{f_{max} - f_{min}}{f_{max} + f_{min}}$$

(27)

where f_{max} and f_{min} stand for the maximum and minimum frequencies of the oscillatory motion, respectively [45].

$$mv = \frac{1}{a_0 + e^{\left(k/2 - k\right)/a_1}}$$

(28)

where a1 and a_0 are two positive numbers used to control exploitation and exploration behavior.

3.4. Movement in the direction of the best white shark

Sharks are able to maintain their position in front of the favorable one, which is close to the prey. This phenomenon is expressed in Equation (29) [45].

$$w_{k+1}^i = w_{gbest_k} + r_1 \times \vec{D}_w \times sgn(r_2 - 0.5) \ r_3 < S_s$$

(29)

where w_{k+1}^i denotes the next position, r1, r2, r3$\in$ to (0,1) and $sgn(r_2 - 0.5)$ control the search direction by providing the values of -1 or
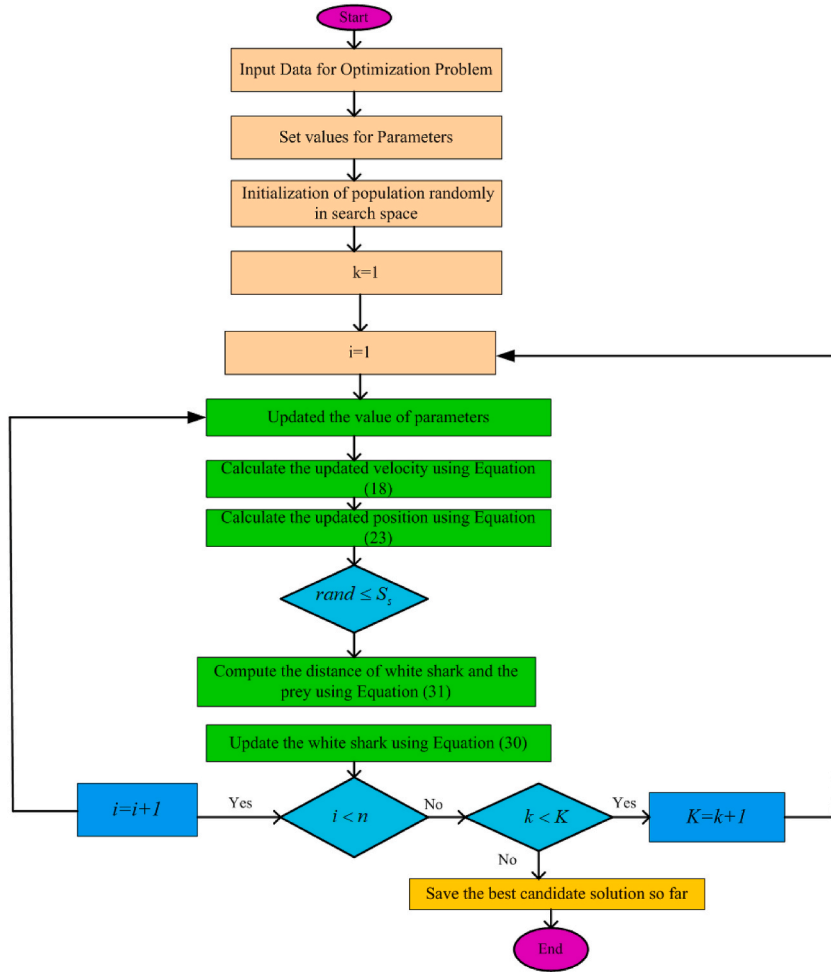
Fig. 4. Flow structure of the proposed WSO algorithm.

1. Equations (30) and (31) represent the distance between shark and prey [45].

$$\overrightarrow{D}_w = \left| rand \times \left(w_{gbest_k} - w_k^i \right) \right| \tag{30}$$

$$S_s = \left| 1 - e^{\left(a2 \times k/K \right)} \right| \tag{31}$$

3.5. Fish school behavior

White shark fish school behavior was defined using Equation (32) [45]:

$$w_{k=1}^i = \frac{w_k^i + w_{k+1}^{'i}}{2 \times rand} \tag{32}$$

WSO behavior is characterized by fish activity and shark migration toward the largest shark, as well as heightened local and global search skills. The flow chart for the proposed WSO algorithm is given in Fig. 4.

4. Proposed control structure

PID controllers can lead to increased stability and quicker controller response. As a result of the derivative mode, the plant receives unreasonably high control inputs. In this case, the noise in the control signals is the primary culprit. Filtering is included in the derivative part to remove injected noise. Fine adjustment the pole can lower noise chattering [50]. Therefore, in the suggested controller,
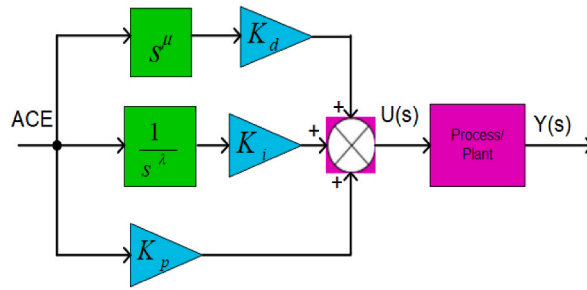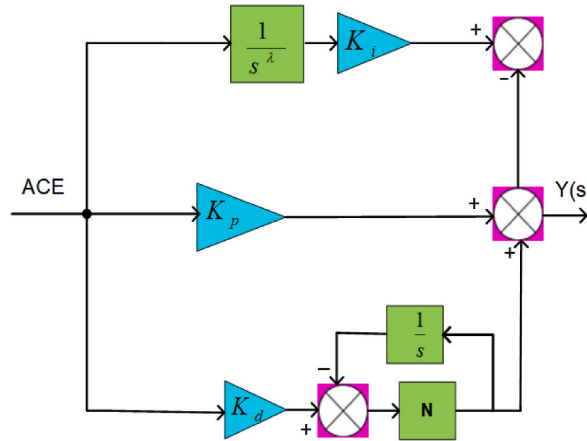
Fig. 5. Configuration of FOPID controller.

Fig. 6. Configuration of FOI-PDN controller.

Table 1
Comparative presentation of various performance metrics.

Techniques	Performance Indices (J)			
	IAE I SE ITAE ITSE			
FO-IPDN: WSO	0.0175	0.000812	0.000045	**0.000070**
FO-IPDN: SSA	0.0134	0.009110	0.000650	**0.000220**
FO-IPDN: FDO	0.0129	0.002230	**0.000100**	0.000140
FO-IPDN: SCA	0.9860	0.009340	0.004710	**0.003590**

Table 2
Techniques for obtaining optimal values.

Gains	Scenario-2				Scenario −3		
	WSO	SSA	FDO	SCA	PID	FOPID	FOI-PDN
K_{p1}	1.993	1.877	1.45	1.998	1.290	1.405	1.893
K_{i1}	1.009	1.458	1.340	1.678	0.232	1.012	1.032
K_{d1}	1.101	1.120	1.543	1.989	0.010	1.890	1.024
λ_1	0.988	0.556	0.620	0.710	0.590	0.786	0.610
μ_1	0.989	0.601	0.823	0.671	0.602	0.644	0.567
N_1	9.760	3.234	9.972	8.678	–	–	9.899
K_{p2}	1.760	1.234	2.000	1.678	1.200	1.232	1.767
K_{i2}	1.120	1.543	1.989	1.010	1.030	1.010	1.012
K_{d1}	1.456	0.220	0.110	1.900	0.010	1.890	1.890
μ_2	0.988	0.456	0.620	0.710	0.503	0.402	0.910
λ_2	0.634	0.972	0.678	0.878	0.671	0.913	0.644
N_2	8.223	9.897	7.89	9.900	–	–	4.456
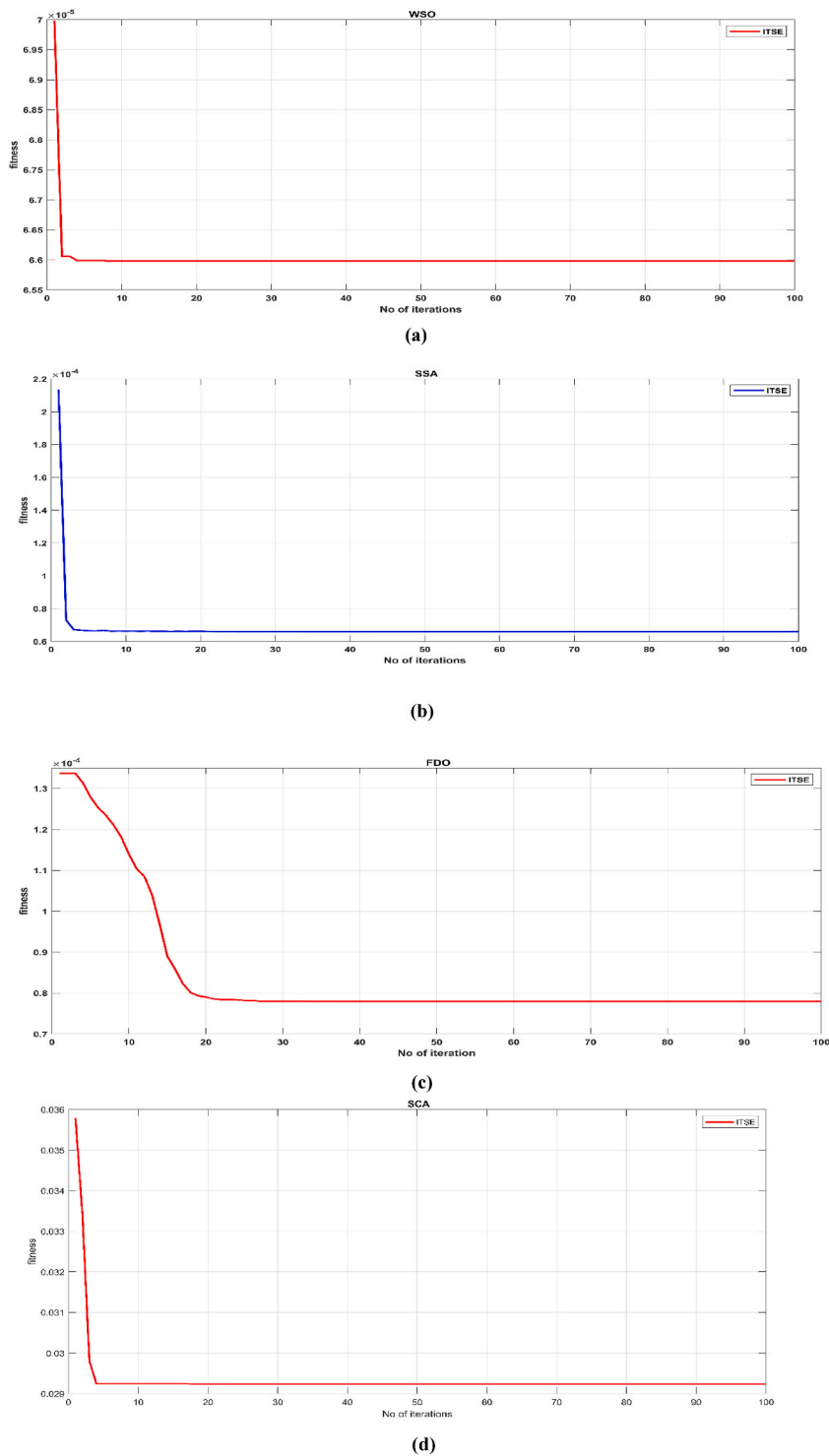
Fig. 7. Convergence profile for algorithms (a) WSO (b) SSA (c) FDO (d) SCA.

the FOI-PDN is chosen to enhance the efficacy of the control methodology. The configurations for FOPID and FOI-PDN are shown in Figs. 5 and 6 respectively. Equations (33)–(35) show the transfer function of FOPID, FOPIDN and FOI-PDN controllers respectively.

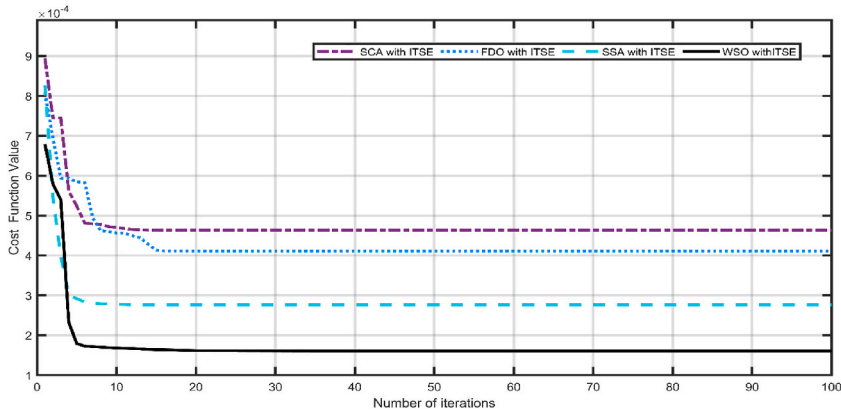$$FOPID = K_p + \frac{K_i}{s^\lambda} + K_d s^\mu \tag{33}$$

Fig. 8. Combined convergence curve for various algorithms.

$$FOPIDN = K_p + \frac{K_i}{s^\lambda} + K_d s^\mu \left[\frac{N_d s}{s + N_d} \right] \tag{34}$$

$$FOPIDN = \frac{K_i}{s^\lambda} - \left\{ K_p + K_d \left[\frac{N_d s}{s + N_d} \right] \right\} \tag{35}$$

In the literature, four distinct performance indices, namely ITSE, ITAE, IAE, and ISE, have been employed. However, in the context of LFC issues, ITAE [2,22,34,35], ITSE [3,17,32,33], and ISE [1,48,49,55] are commonly utilized. To compare these performance indices for our proposed power system, equations (36)–(39) were implemented in MATLAB. The results, presented in Table 1, indicate that the minimum fitness error was achieved for ITSE in comparison to ITAE, ISE, and IAE.

$$ITSE = J_1 = \int_0^t t \left[\Delta F_1^2 + \Delta F_2^2 + \Delta P_{tie}^2 \right] dt \tag{36}$$

$$ITAE = J_2 = \int_0^t t [\Delta F_1 + \Delta F_2 + \Delta P_{tie}] dt \tag{37}$$

$$ISE = J_3 = \int_0^t \left[\Delta F_1^2 + \Delta F_2^2 + \Delta P_{tie}^2 \right] dt \tag{38}$$

$$IAE = J_4 = \int_0^t t [\Delta F_1 + \Delta F_2 + \Delta P_{tie}] dt \tag{39}$$

The constraints used in Equation (40) represent the controller coefficients for FOPID and FOI-PDN.

$$K_p^{Min} \le K_p \le K_p^{Max}; \ K_d^{Min} \le K_d \le K_d^{Max}; \ K_i^{Min} \le K_i \le K_i^{Max}; \ \lambda^{Min} \le \lambda \le \lambda^{Max}; \ N_d^{Min} \le N_d \le N_d^{Max}; \ \mu^{Min} \le \mu \le \mu^{Max} \tag{40}$$

5. Results and discussion

This section examines the efficacy and validation of the FOI-PDN controller execution. For fair comparison, a newly proposed WSO algorithm was used to regulate the several control parameters of FOI-PDN and other controllers including PID and FOPID. With the use of the Simulink tool of the investigated PS, the WSO method was developed using the MATLAB system's m-file code. The optimized WSO-based controller coefficients are shown in Table 2. The proposed FOI-PDN controller's robustness is evaluated by comparing it to PID and FOPID controllers. The following scenarios examine the findings for the analyzed multi-area IPS in various case studies.

5.1. Scenario-1

In this scenario, the convergence profile for different algorithms such as WSO, SSA, SCA and FDO have been evaluated for hybrid interconnected PS and as show in Fig. 7(a–d). The coefficients of the proposed FOI-PDN controller are regulated using the ITSE tests as a CF. To achieve the optimal controller gains, the WSO parameter values from (Appendix A) were chosen. With each optimization technique having 20 populations, a total of 30 runs are simulated with 100 repetitions and the excess of the factors are given (Appendix B). Fig. 7(a–d) shows that the proposed WSO optimization process exhibits better and faster conversion characteristics for ITSE objective functions than the investigated FDO, SSA, and SCA optimizers. Fig. 7(a–d) shows that the WSO technique converges swiftly under the ITSE circumstances and achieves (ITSE = 0.000070) associated to SSA, FDO, and SCA, which have respective ITSE
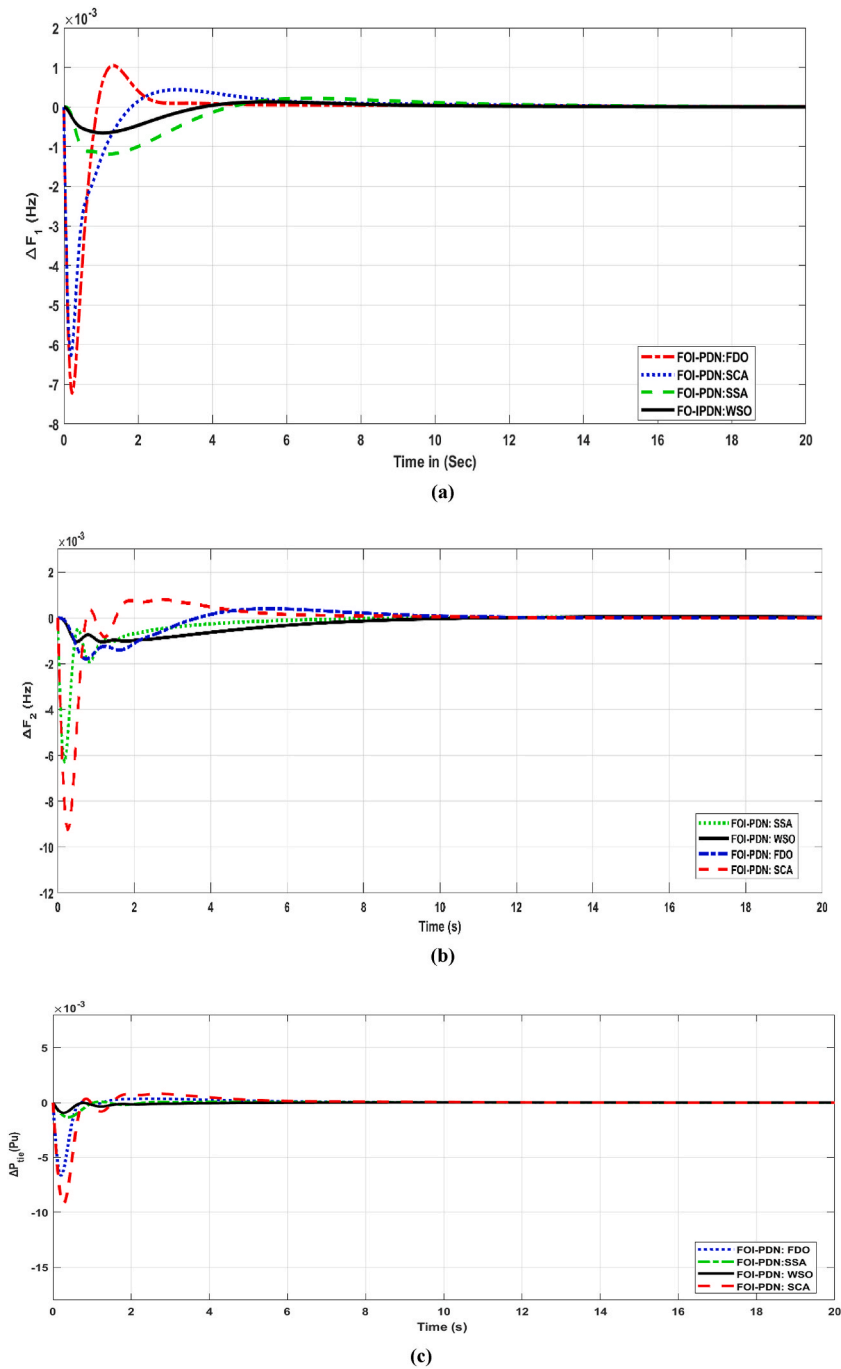
Fig. 9. Dynamic response of the system for scenario-2 (a) ΔF_1 (b) ΔF_2 (c) ΔP_{tie}.

values of 0.000220, 0.000140, and 0.00359, respectively. The combined convergence diagram for Fig. 7(a–d) is shown in Fig. 8.

5.2. Scenario-2

In this scenario, the efficiency of the proposed WSO algorithm has been compared with other recent optimizer algorithms such as SSA, FDO and SCA employed for two area hybrids interconnected PS. The response for each technique has been assessed for interconnected tie line ΔP_{tie}), area 2 (ΔF_2), and area-1 (ΔF_1) and as depicted in Fig. 9(a–c). The comparison for different optimization algorithms in respect of transient contents including maximum overshoot (MO), minimum undershoot (MU) and Settling time (ST) with a band of 0.005% are displayed in Table-3 for (ΔF_1), (ΔF_2) and (ΔP_{tie}). It can be observed from Table-3 and Fig. 9(a–c) that our

Table 3
Transient outcomes for PS considering scenario 2.

| Controller with Algorithms	ST (Settling time)			MO (Maximum Overshoot)			MU (Minimum Undershoot)		
	ΔF_1	ΔF_2	ΔP_{tie}	ΔF_1	ΔF_2	ΔP_{tie}	ΔF_1	ΔF_2	ΔP_{tie}
FOI-PDN (WSO)	6.82	9.93	**4.420**	0.000129	**0.000041**	**0.000017**	−0.00065	−0.00104	−0.00094
FOI-PDN (SSA)	12.6	**6.23**	5.020	0.000218	0.000048	0.000082	−0.00119	−0.00628	−0.00135
FOI-PDN (SCA)	8.83	8.61	6.533	0.000437	0.000406	0.000363	−0.00627	−0.00179	−0.00664
FOI-PDN (FDO)	**5.98**	10.9	8.434	0.001045	0.000813	0.000813	−0.00722	−0.00922	−0.00922
[52] MID (hDE-PS)	19.0	18.09	12.69	0.000800	0.001700	0.000600	−0.00100	−0.01500	−0.00800
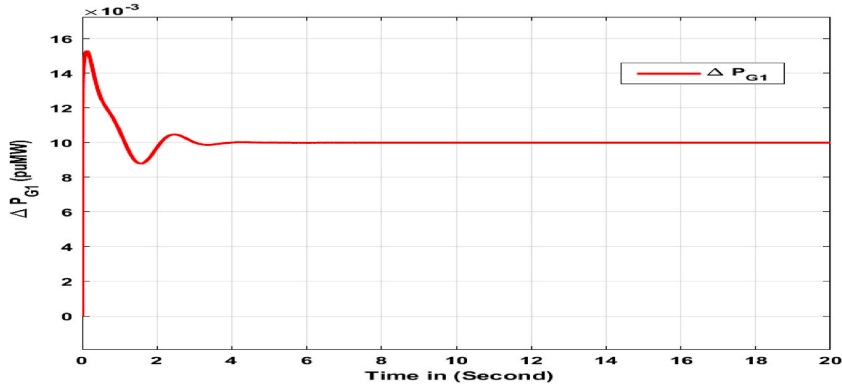
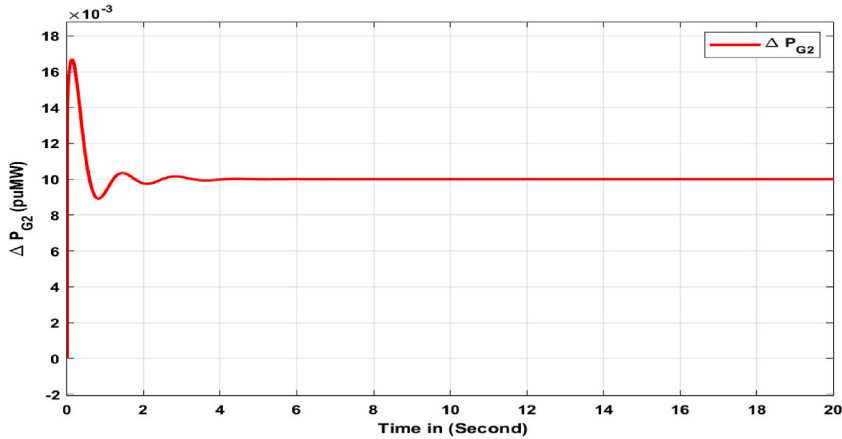**Fig. 10.** Output power for all the generation units in area 1.

Fig. 11. Output power for all the generation units in area 2.

proposed algorithm excellently performs in terms of MU and MS for interrelated tie line (ΔP_{tie}), area 2 (ΔF_2), and area-1 (ΔF_1) as compared to SSA, SCA, hDE with PS, and FDO algorithms. Furthermore, it can also be observed that the settling time for FDO algorithms (ST = 5.98) for area-1 has the lowest value as compared to SSA (ST = 6.82), SCA (ST = 8.83), SSA (12.8), and hDE-PS (ST = 19.0) while the next position is occupied by WSO algorithms. Similarly for area-1 the minimum undershoots, and overshoot is observed for our proposed WSO algorithm (MO = 0.00129, MU = −0.00065) as compared to SSA (MU = −0.00119, MO = 0.000118), FDO (MU = −0.00627, MO = 0.000437), SCA (MO = 0.001045, MU = −0.00722), hDE-PS (MO = 0.000800, MU = −0.00100). In area-2 the settling time for SSA algorithms (ST = 6.23) has the lowest value as compared to WSA (ST = 6.82), SCA (ST = 9.93), FDO (10.8), and hDE-PS (ST = 18.09) but in this area −2 the MO and MU for the proposed WSA superiorly perform as compared to the rest of other mentioned algorithms. The output power for all the generation units considering area-1 and area-2 is shown in Figs. 10 and 11 respectively. Moreover, the proposed approach also performs very well in respect of MU, ST, and MO for interconnected tie-line as compared to SSA, SCA, FDO and hDE-PS.
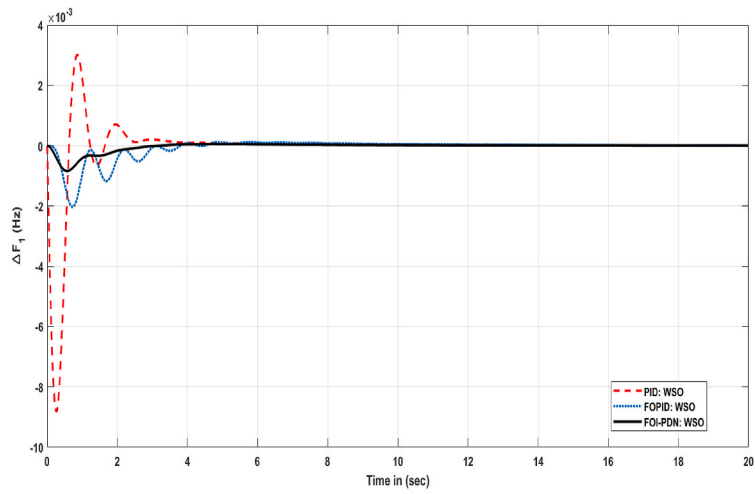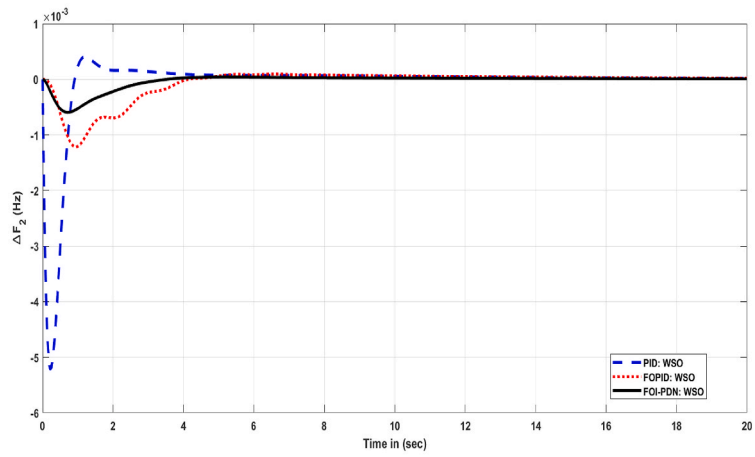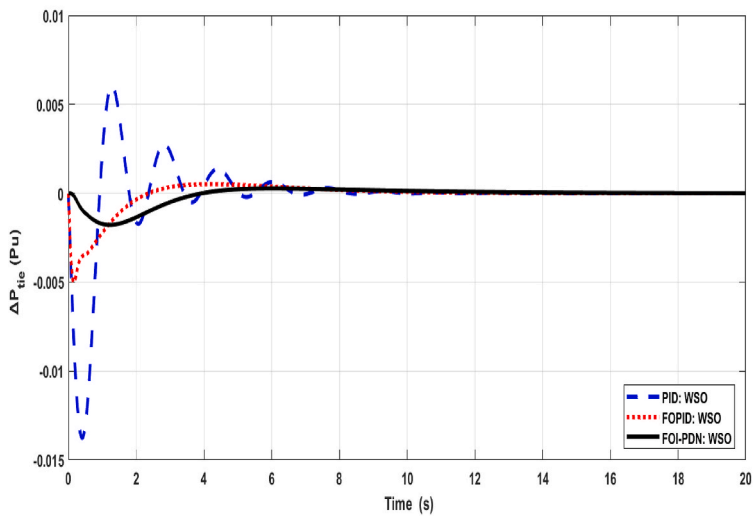
Fig. 12. Dynamic response of the system for scenario-3 (a) ΔF_1 (b) ΔF_2 (c) ΔP_{tie}.

Table 4
Transient outcomes for PS considering scenario 3.

Controller with Algorithms	ST (Settling time)			MO (Maximum Overshoot)			MU (Minimum Undershoot)		
	ΔF_1	ΔF_2	ΔP_{tie}	ΔF_1	ΔF_2	ΔP_{tie}	ΔF_1	ΔF_2	ΔP_{tie}
FOI-PDN (WSO)	2.96	8.23	3.93	0.000000	0.000272	0.000041	−0.00084	−0.00178	−0.00059
FOPID (WSO)	7.83	8.46	8.09	0.000127	0.000509	0.000090	−0.00202	−0.00500	−0.00121
PID (WSO)	4.68	10.4	5.91	0.003012	0.006035	0.000402	−0.00883	−0.01376	−0.00521
[52] (hDE-PS)	19.0	18.09	12.69	0.000800	0.001700	0.000600	−0.00100	−0.01500	−0.00800
[23] FOTID (FPA)	25.5	23.2	18.77	0.00680	0.01170	0.00260	−0.02450	−0.0228	−0.00440
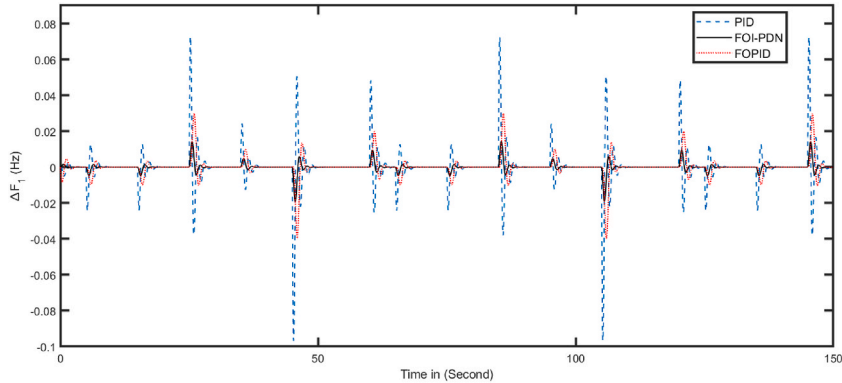
Fig. 13. Random variation for the consider power system employing various controllers.

5.3. Scenario-3

In this case, the performance of FOPID, MID, FOTID, and PID controllers was compared to the efficiency of a FOI-PDN controller tuned with the WSO technique. The dynamic response for different techniques has been depicted in Fig. 12(a–c) for connected tie line (ΔP_{tie}), area 2 (ΔF_2), and area-1 (ΔF_1). The overall, comparison in respect of MU, MO and ST are displayed in Table-4 for (ΔF_1), (ΔF_2) and (ΔP_{tie}). Fig. 12(a–c) shows that the FO-IPDN controller adjusted with the WSO methods has an amended ST of 31.56% for (ΔF_1) and 29.22% for (ΔF_2), but nearly the identical highest overshoot as the FOPID adjusted with the WSO methods. Table-4 shows that for (ΔF_1), (ΔF_2), and (ΔP_{tie}), the FOI-PDN controller with the WSO-adjusted approach works better than the FOPID controller optimized with WSO techniques in terms of ST (13.01%, 29.40%, and 45.63%) and MO (89.12%, 83.11%, and 98.10%). Considering (ΔF_1), (ΔF_2), and (ΔP_{tie}), respectively, the FOI-PDN controller significantly reduced peak overshoot by 73.33%, 91.03%, and 77.21% when associated to a PID controller adjusted with similar methods. From Table 4 it can be clearly observed that our proposed FOI-PDN controller optimized with WSO superiorly perform as compared to FOPID and PID controllers optimized with the same approach, MID controller [52] optimized with hDE-PS, FOTID controller adjusted with FPA [23] for interrelated tie line (ΔP_{tie}), area 2 (ΔF_2), and area-1 (ΔF_1). The system's performance under the influence of randomly varying loads (± 0.10, ± 0.15, ± 0.25, ± 0.3, ± 0.4, ± 0.5 pu) for a simulation period of 150 s has been illustrated in Fig. 13, employing various controllers in the presence of an electric vehicle (EV). As observed in Fig. 13, the proposed FOI-PDN controller based on WSO continues to demonstrate superior response to random load fluctuations. It exhibits lower steady-state error, faster response times, and better-damped variations compared to contemporary controllers.

5.4. Sensitivity, robustness and stability analysis

The supplied controller must perform reliably under parameter uncertainties due to its versatile mathematical illustration of system representations and the likelihood that system parameters and arrangement may alter over time due to component wear and tear. When the suggested control structure is unable to handle the system parametric uncertainties, these uncertainties can occasionally cause difficulties with the system's stability. To confirm the sturdiness of the suggested FOI-PDN controller, different values of parameters such as Tg, R, B, and T_{12} are altered by approximately ± 30% and compared to their nominal parameter response. Fig. 14(a and b) and Table-5 display the findings that were obtained when system parameter fluctuations were used, demonstrating the proposed controller's reliability in the appearance of constraint uncertainty. In addition, the nature of the load in an actual power system is unpredictable and variable. The control method must be able to accommodate random load fluctuations. Consequently, the resilience of the suggested controller is observed despite varying loads. In order to simulate real-time scenarios, the performance of the WSO: FOI-PDN controller is validated under various load disruptions up to (± 25% and ± 50%) and is given in Fig. 15. Table- 5 shows that several parameters respond close to their nominal levels. This demonstrates that the proposed WSO-based FOI-PDN controller provides dependable execution throughout a range of ± 30% of the system parameters. In addition, the optimal values of the proposed
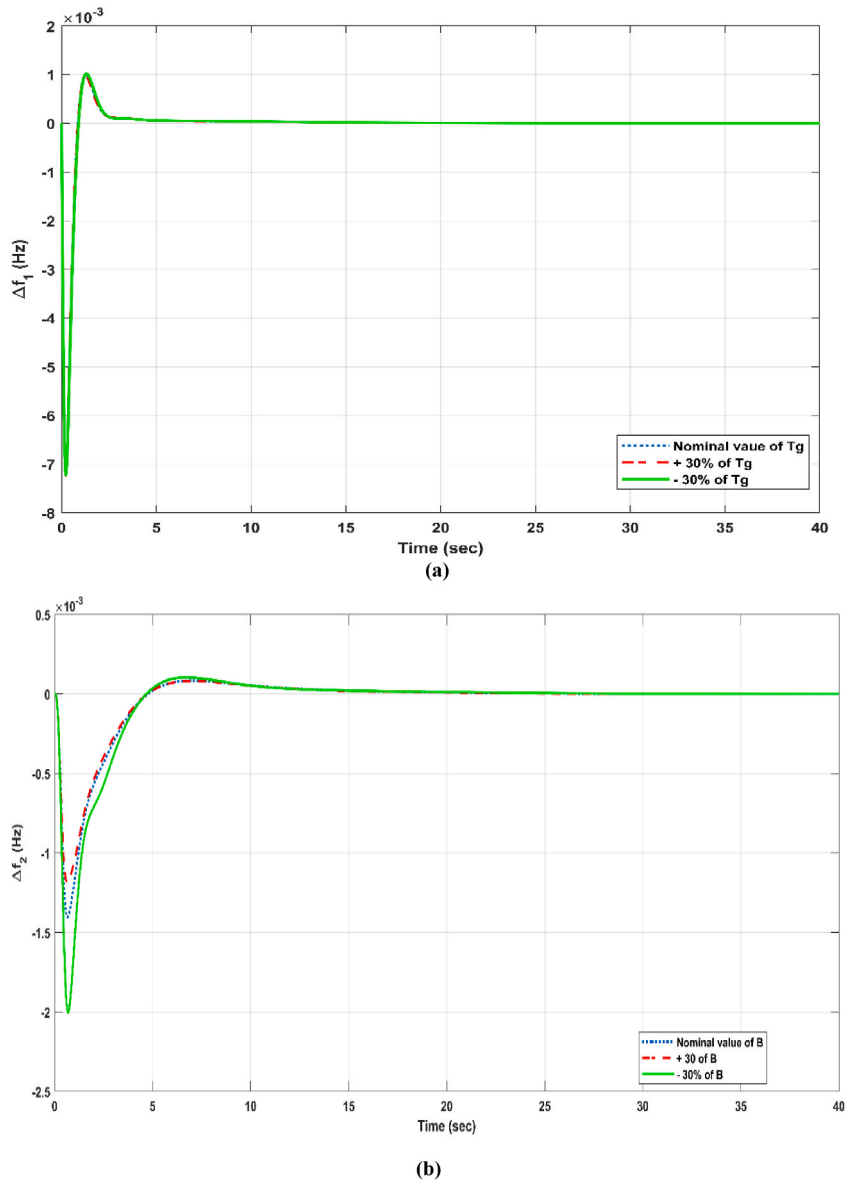
(a)

(b)

Fig. 14. Sensitivity analysis for the system parameters considering (a) Tg (b) B.

Table 5
Power system transient response computation.

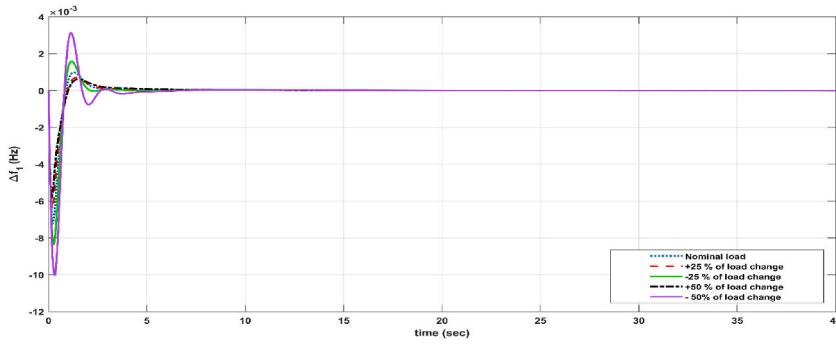| Parameter	% Change	ST			MO			MU		
		ΔF_1	ΔF_2	ΔP_{tie}	ΔF_1	ΔF_2	ΔP_{tie}	ΔF_1	ΔF_2	ΔP_{tie}
T_g	+30	3.47	12.72	14.09	0.000323	0.00068	0.00064	−0.00315	−0.00240	−0.00610
	−30	3.51	12.73	14.10	0.000276	0.00047	0.00054	−0.00313	−0.00236	−0.00600
B	+30	6.38	13.45	14.21	0.000296	0.00037	0.00094	−0.00489	−0.00713	−0.00693
	−30	8.03	13.46	14.23	0.000289	0.00030	0.00098	−0.00482	−0.00913	−0.00678
R	+30	6.10	12.79	14.60	0.000310	0.00014	0.00083	−0.00361	−0.00780	−0.00731
	−30	7.80	12.80	14.61	0.000311	0.00017	0.00075	−0.00361	−0.00740	−0.00725
T_{12}	+30	6.09	13.23	14.89	0.00031	0.00032	0.00063	−0.00251	−0.00830	−0.00623
	−30	7.82	13.23	14.90	0.00032	0.00031	0.00061	−0.00257	−0.00840	−0.00618

Fig. 15. System load changes.
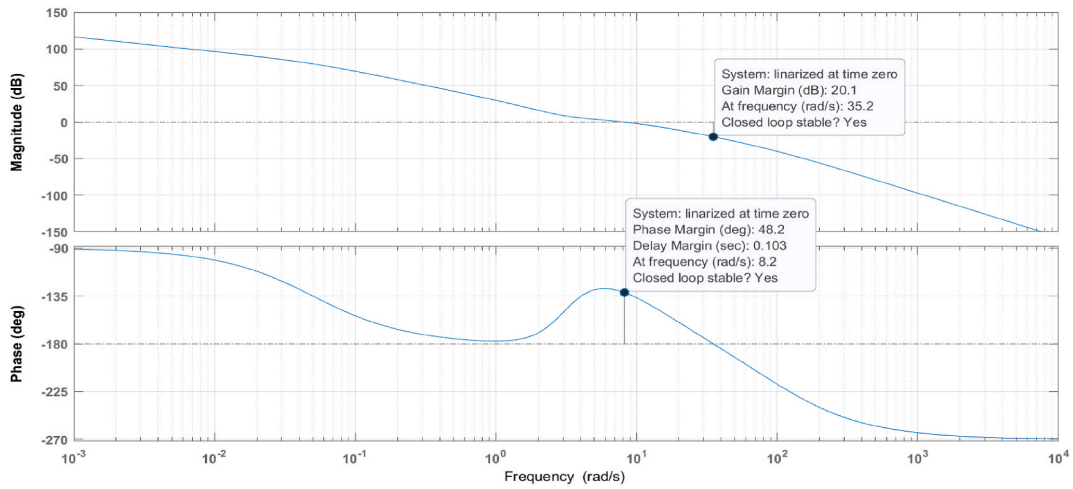
Fig. 16. Bode diagram for the consider power system.

controller do not require retuning for a broad range of parameters at rated value with actual parameters. Furthermore, the stability of the system using the suggested FOI-PDN controller is illustrated through the Bode diagram, as depicted in Fig. 16. As depicted in Fig. 16, the phase margin (PM), gain crossover frequency (ω_{gc}), gain margin (GM), and phase crossover frequency (ω_{pc}) are determined to be 48.2°, 8.2 rad/s, 20.1 dB, and 35.2 rad/s respectively. Since both GM and PM are positive, with PM greater than GM, and ω_{gc} less than ω_{pc}, which indicates that the system is stable.

6. Conclusion and future study

The present study proposes an FOI-PDN controller to control the LFCs of dual regions with hybrid renewable energies and conventional energy sources using several nonlinearities such as GDZ, GRC, CTD, and BD. The settings of the suggested controller were optimized using the modern and potent metaheuristic algorithm known as the White Shark Optimizer (WSO). The simulation outcomes demonstrate that the WSO-based tuned FOI-PDN controller successfully reduces peak overshoot by 73.33%, 91.03%, and 77.21% for region-2, region-1, and link power variation respectively, and delivers MU of 89.12%, 83.11%, and 78.10% for both regions and link power. Likewise, the WSO based FOI-PDN controller enhances the ST by 13.01%, 29.40%, and 45.63% for the load frequency of (ΔF_1), (ΔF_2), and (ΔP_{tie}) respectively, when compared with the (MID: hDE-PS).The outcome demonstrate that when the system characteristics or load circumstances change, the gains of the proposed controller are not reset. The WSO-based FOI-PDN controller's efficiency demonstrates that it can effectively address LFC issues in hybrid power systems with prolonged oscillations. In the future, the suggested control scheme will be developed and implemented in Matlab Simulink and practically using OPAL-RT simulator with the inclusion of energy storage devices and renewable energies, as well as other proficient controllers like MPC and FLC for the power system.

Data Availability

Data used to support the findings of this study is included within the article.

CRediT authorship contribution statement

Amil Daraz: Writing – original draft, Validation, Software, Methodology, Formal analysis, Data curation, Conceptualization. **Irfan Ahmed Khan:** Software, Resources, Investigation, Data curation. **Abdul Basit:** Writing – review & editing, Visualization, Methodology. **Suheel Abdullah Malik:** Writing – review & editing, Validation, Supervision, Formal analysis, Conceptualization. **Salman A. Alqahtani:** Writing – review & editing, Funding acquisition, Conceptualization. **Guoqiang Zhang:** Writing – review & editing, Visualization, Supervision, Project administration.

Declaration of competing interest

The authors declare that they have no known competing financial interests or personal relationships that could have appeared to influence the work reported in this paper.

Acknowledgments

Appendix A

LFC model			
Parameter	Value	Parameter	Value
K_p	68.97	T_p	11.49
a_{12}	−1	R_H	2.4
B_1	0.4312	R_T	2.4
B_2	0.4312	P_{r1}, Pr2 (MW)	1000
Reheat Thermal generation			
T_{tr}	0.3	K_T	0.895
K_{re}	0.3	T_{re}	10
		T_{gr}	0.08
Electric Vehicles			
C_{nom}	66.2	V_{nom}	364.8
R_t	0.047	R_s	0.074
RT/F	0.02612	C_t	703.6
Maximum SOC (in Percentage)	95	Minimum SOC (in Percentage)	10
C_{nom}	66.2	C_{Batt}	24.15
K_{EVE1}	0.005	K_{EVE2}	0.005
Hydro Power generation			
T_{rh}	28.749	T_w	1
Tr	5	Kh	0.32586
T_{gh}	0.2		
Renewable energy resources			
K_{PV}	1	T_{PV}	1.3
K_{wind}	0.100	K_{solar}	0.100
T_W	1.5	K_W	1
Boiler Dynamic			
K3	0.92	*Cb*	200
Tf	0.23	Trb	0.545
T_{rh}	28.75	Tr	1.4
K2	0.095	K1	0.85
K1b	0.950	T_{1b}	0.545

Appendix B
WSO terms and their values

Coefficient	Values	Coefficient	Values	Coefficient	Values	Coefficient	Values
No of dimension	7	Lower limit (Lb)	−2	No of Population (Np)	30	Upper limit (Ub)	2
Random Number (r)	[0,1]	Acceleration Coefficient (τ)	4.125				

References

[1] A. Hassan, M. Aly, A. Elmelegi, L. Nasrat, M. Watanabe, E.A. Mohamed, Optimal frequency control of multi-area hybrid power system using new cascaded TID-PI$^\lambda D^\mu$N controller incorporating electric vehicles, Fractal Fract 6 (2022) 548, https://doi.org/10.3390/fractalfract6100548.

[2] K. Singh, M. Dahiya, A. Grover, R. Adlakha, M. Amir, An effective cascade control strategy for frequency regulation of renewable energy based hybrid power system with energy storage system, J. Energy Storage 68 (2023) 107804.

[3] A. Daraz, S.A. Malik, I.U. Haq, K.B. Khan, G.F. Laghari, F. Zafar, Modified PID controller for automatic generation control of multisource interconnected power system using fitness dependent optimizer algorithm, PLoS One 15 (2020) e0242428.

[4] R.K. Khadanga, S. Panda, A modified local input signal for SSSC-based damping controller design, Elec. Power Compon. Syst. 49 (11–12) (2022) 978–989.

[5] A.K. Mishra, Puneet Mishra, H.D. Mathur, Design of a dual-layered tilt frequency control structure for interconnected power system integrated with DFIG, International Transaction on Electrical Energy Systems 31 (Issue 9) (2021).

[6] R.K. Khadanga, S. Padhy, P.R. Sahu, S. Panda, Frequency regulation of a distributed power system via modified whale optimization algorithm, in: 2021 Innovations in Power and Advanced Computing Technologies (I-PACT), IEEE, 2021, November, pp. 1–6.

[7] Z. Hu, S. Liu, L. Wu, Credibility-based distributed frequency estimation for plug-in electric vehicles participating in load frequency control, Int. J. Electr. Power Energy Syst. 130 (2021) 106997.

[8] A. Fernández-Guillamón, E. Gómez-Lázaro, E. Muljadi, Á. Molina-García, Power systems with high renewable energy sources:A review of inertia and frequency control strategies over time, Renew. Sustain. Energy Rev. 115 (2019) 109369.

[9] Y. Arya, Effect of electric vehicles on load frequency control in interconnected thermal and hydrothermal power systems utilizing CFFOIDF controller, IET Gener. Transm. Distrib. 14 (2020) 2666–2675.

[10] X. Lv, Y. Sun, Y. Wang, V. Dinavahi, Adaptive Event-triggered load frequency control of multi-area power systems under networked environment via sliding mode control, IEEE Access 8 (2020) 86585–86594.

[11] K. Vrdoljak, N. Perić, I. Petrović, Sliding model based load-frequency control in power systems, Electr. Power Syst. Res. 80 (2010) 514–527.

[12] C. Pan, C. Liaw, An adaptive controller for power system load-frequency control, IEEE Trans. Power Syst. 4 (1989) 122–128.

[13] Y. Arya, N. Kumar, BFOA-scaled fractional order fuzzy PID controller applied to AGC of multi-area multi-source electric power generating systems, Swarm Evol. Comput. 32 (2017) 202–218.

[14] R.K. Khadanga, A. Kumar, S. Panda, A novel modified whale optimization algorithm for load frequency controller design of a two-area power system composing of PV grid and thermal generator, Neural Comput. Appl. 32 (12) (2020) 8205–8216.

[15] M.S. Ayas, E. Sahin, FOPID controller with fractional filter for an automatic voltage regulator, Comput. Electr. Eng. 90 (2021) 106895.

[16] D. Yousri, T.S. Babu, A. Fathy, Recent methodology-based Harris Hawks optimizer for designing load frequency control incorporated in multi-interconnected renewable energy plants, Sustain. Energy Grids Netw. 22 (2020) 100352.

[17] A. Daraz, S.A. Malik, A.T. Azar, S. Aslam, T. Alkhalifah, F. Alturise, Optimized fractional order integral-tilt derivative controller for frequency regulation of interconnected diverse renewable energy resources, IEEE Access 10 (2022) 43514–43527.

[18] A. Oshnoei, R. Khezri, S.M. Muyeen, S. Oshnoei, F. Blaabjerg, Automatic generation control incorporating electric vehicles, Elec. Power Compon. Syst. 47 (2019) 720–732.

[19] G. Magdy, A. Bakeer, M. Nour, E. Petlenkov, A new virtual synchronous generator design based on the SMES system for frequency stability of low-inertia power grids, Energies 13 (21) (Oct. 2020) 5641.

[20] G. Zhang, A. Daraz, I.A. Khan, A. Basit, M.I. Khan, M. Ullah, Driver training based optimized fractional order PI-pdf controller for frequency stabilization of diverse hybrid power system, Fractal Fract 7 (2023) 315.

[21] Mausri Bhuyan, Dulal Chandra Das, Amar Kumar Barik, Subash Chandra Sahoo, Performance assessment of novel solar thermal-based dual hybrid microgrid system using CBOA optimized cascaded PI-TID controller, IETE J. Res. (2022), https://doi.org/10.1080/03772063.2022.2083026.

[22] Y. Arya, Impact of ultra-capacitor on automatic generation control of electric energy systems using an optimal FFOID controller, Int. J. Energy Res. 43 (14) (Aug. 2019) 8765–8778, https://doi.org/10.1002/er.4767.

[23] S. Priyadarshani, K.R. Subhashini, J.K. Satapathy, ℙPath finder algorithm optimized fractional order tilt-integral-derivative (FOTID) controller for automatic generation control of multi-source power system, Microsyst. Technol. 27 (1) (Jun. 2020) 23–35.

[24] S.C. Sahoo, A.K. Barik, D.C. Das, A novel Green Leaf-hopper Flame optimization algorithm for competent frequency regulation in hybrid microgrids, Int J Numer Model 35 (3) (2022) e2982, https://doi.org/10.1002/jnm.2982.

[25] I. Eke, M. Saka, H. Gozde, Y. Arya, M.C. Taplamacioglu, Heuristic optimization based dynamic weighted state feedback approach for 2DOF PI-controller in automatic voltage regulator, Engineering Science and Technology, Int. J. 24 (Issue 4) (2021) 899–910, https://doi.org/10.1016/j.jestch.2020.12.023.

[26] T.K. Mohapatra, A.K. Dey, B.K. Sahu, Employment of quasi oppositional SSA-based two-degree-of-freedom fractional order PID controller for AGC of assorted source of generations, IET Gener. Transm. Distrib. 14 (2020) 3365–3376, https://doi.org/10.1049/iet-gtd.2019.0284.

[27] S. Malik, S. Suhag, A novel SSA tuned PI-tdf control scheme for mitigation of frequency excursions in hybrid power system, Smart Sci 8 (2020) 202–218.

[28] A. Elmelegi, E.A. Mohamed, M. Aly, E.M. Ahmed, A.A.A. Mohamed, O. Elbaksawi, Optimized tilt fractional OrderCooperative controllers for preserving frequency stability in renewable energy-based power systems, IEEE Access 9 (2021) 8261–8277.

[29] Y. Arya, A new optimized fuzzy FOPI-FOPD controller for automatic generation control of electric power systems, J. Frankl. Inst. 356 (2019) 5611–5629.

[30] Y. Arya, Improvement in automatic generation control of two-area electric power systems via a new fuzzy aided optimal PIDN-FOI controller, ISA Trans. 80 (2018) 475–490.

[31] M. Bhuyan, D.C. Das, A.K. Barik, Proficient power control strategy for combined solar gas turbine-wind turbine generator-biodiesel generator based two area interconnected microgrid employed with DC link using Harris's hawk optimization optimised tilt-integral-derivative controller, Int J Numer Model 35 (4) (2022) e2991, https://doi.org/10.1002/jnm.2991.

[32] A. Daraz, S.A. Malik, H. Mokhlis, I.U. Haq, F. Zafar, N.N. Mansor, "Improved-Fitness dependent optimizer based FOI-PD controller for automatic generation control of multi-source interconnected power system in deregulated environment", IEEE Access 8 (2020) 197757–197775, https://doi.org/10.1109/ACCESS.2020.3033983.

[33] A. Daraz, S.A. Malik, A. Basit, S. Aslam, G. Zhang, Modified FOPID controller for frequency regulation of a hybrid interconnected system of conventional and renewable energy sources, Fractal Fract. 7 (2023) 89, https://doi.org/10.3390/fractalfract7010089.

[34] Y. Arya, "Impact of hydrogen Aqua electrolyzer-fuel cell units on automaticgeneration control of power systems with a new optimal fuzzy TIDFII controller, Renew. Energy 139 (Aug. 2019) 468_482.

[35] K. Singh, Y. Arya, Jaya-ITDF control strategy based frequency regulation of multi microgrid utilizing energy stored in high voltage direct current-link capacitors, Soft Comput. 27 (2023) 5971, https://doi.org/10.1007/s00500-023-08044-9.

[36] Ravi Choudhary, J.N. Rai, Yogendra Arya, Cascade FOPI-FOPTID controller with energy storage devices for AGC performance advancement of electric power systems, Sustain. Energy Technol. Assessments 53 (2022) 102671, https://doi.org/10.1016/j.seta.2022.102671. Part C.

[37] Kavita Singh, Yogendra Arya, Tidal turbine support in microgrid frequency regulation through novel cascade Fuzzy-FOPID droop in de-loaded region, ISA Trans. 133 (2023) 218–232.

[38] Jyoti Ranjan Nayak, Binod Shaw, Binod Kumar Sahu, Karanam Appala Naidu, Application of optimized adaptive crow search algorithm based two degree of freedom optimal fuzzy PID controller for AGC system, Engineering Science and Technology, an International Journal 32 (2022) 101061, https://doi.org/10.1016/j.jestch.2021.09.007.

[39] A. Daraz, S.A. Malik, A. Waseem, A.T. Azar, I.U. Haq, Z. Ullah, S. Aslam, Automatic generation control of multi-source interconnected power system using FOI-TD controller, Energies 14 (2021) 5867, https://doi.org/10.3390/en14185867.

[40] Hany M. Hasanien, Attia A. El-Fergany, "Salp swarm algorithm-based optimal load frequency control of hybrid renewable power systems with communication delay and excitation cross-coupling effect.", Elec. Power Syst. Res. 176 (2019) 105938 https://doi.org/10.1016/j.epsr.2019.105938.

[41] A. Latif, S.M.S. Hussain, D.C. Das, T.S. Ustun, "Optimum synthesis of a BOA optimized novel dual-stage PI-(1 C ID) controller for frequency response of a microgrid,'', Energies 13 (13) (Jul. 2020) 3446.

[42] Y. Arya, N. Kumar, P. Dahiya, G. Sharma, E. Çelik, S. Dhundhara, M. Sharma, "Cascade-IDN controller design for AGC of thermal and hydro-thermal power systems integrated with renewable energy sources, IET Renew. Power Gener., early access (Jan. 2021) 1_17, https://doi.org/10.1049/rpg2.12061.

[43] M. Khamies, G. Magdy, A. Selim, S. Kamel, An improved Rao algorithm for frequency stability enhancement of nonlinearpower system interconnected by AC/DC links with high renewables penetration, Neural Comput. Appl. 34 (2021) 2883–2911, 56.

[44] A.H.A. Elkasem, S. Kamel, M.H. Hassan, M. Khamies, E.M. Ahmed, An eagle strategy arithmetic optimization algorithm for frequency stability enhancement considering high renewable power penetration and time-varying load, Mathematics 10 (2022) 854.

[45] B. Malik, H. Abdelaziz, A. Jaffar, A. Mohammed, A. Betar, A.A. Mohammed, White Shark Optimizer: a novel bio-inspired meta-heuristic algorithm for global optimization problems, Knowl. Base Syst. 243 (2022) 108457, https://doi.org/10.1016/j.knosys.2022.108457.

[46] M.A. Ali, S. Kamel, M.H. Hassan, E.M. Ahmed, M. Alanazi, Optimal power flow solution of power systems with renewable energy sources using white sharks algorithm, Sustainability 14 (2022) 6049, https://doi.org/10.3390/su14106049.

[47] S.N. Makhadmeh, M.A. Al-Betar, K. Assaleh, S. Kassaymeh, A hybrid white shark equilibrium optimizer for power scheduling problem based IoT, IEEE Access 10 (2022) 132212–132231, https://doi.org/10.1109/ACCESS.2022.3229434.

[48] E.M. Ahmed, E.A. Mohamed, A. Elmelegi, M. Aly, O. Elbaksawi, Optimum modified fractional order controller for FutureElectric vehicles and renewable energy-based interconnected power systems, IEEE Access 9 (2021) 29993–30010.

[49] E.A. Mohamed, E.M. Ahmed, A. Elmelegi, M. Aly, O. Elbaksawi, A.A.A. Mohamed, An optimized hybrid fractional order controller for frequency regulation in multi-area power systems, IEEE Access 8 (2020) 213899–213915.

[50] T. Ali, S.A. Malik, A. Daraz, S. Aslam, T. Alkhalifah, Dandelion optimizer-based combined automatic voltage regulation and load frequency control in a multi-area, multi-source interconnected power system with nonlinearities, Energies 15 (2022) 8499.

[51] W. Tasnin, L.C. Saikia, M. Raju, Deregulated AGC of multi-area system incorporating dish-Stirling solar thermal and geothermalpower plants using fractional order cascade controller, Int. J. Electr. Power Energy Syst. 101 (2018) 60–74.

[52] R. Sahu, T. Gorripotu, S. Panda, A hybrid DE-PS algorithm for load frequency control under deregulated power system withUPFC and RFB, Ain Shams Eng. J. 6 (2015) 893–911.

[53] A. Daraz, S. Abdullah, H. Mokhlis, I.U. Haq, G. Fareed, N.N. Mansor, Fitness dependent optimizer-based automatic generation control of multisource interconnected power system with non-linearities, IEEE Access 8 (2020) 100989–101003.

[54] P.K. Ray, S.R. Mohanty, N. Kishor, Proportional–integral controller based small-signal analysis of hybrid distributed generation systems, Energy Convers. Manag. 52 (2011) 1943–1954.

[55] E.M. Ahmed, A. Selim, H. Alnuman, W. Alhosaini, M. Aly, E.A. Mohamed, Modified frequency regulator based on ti^{λ}-tdμff controller for interconnected microgrids with incorporating hybrid renewable energy sources, Mathematics 11 (2023) 28, https://doi.org/10.3390/math11010028.

[56] D. Kumar, H.D. Mathur, S. Bhanot, R.C. Bansal, Frequency regulation in islanded microgrid considering stochastic model of wind and PV, Int Trans Electr Energ Syst 29 (2019) e12049, https://doi.org/10.1002/2050-7038.12049.